JOURNAL OF MATERIALS SCIENCE 28 (1993) 5456–5460

Aqueous precipitation and electrical properties of In_2S_3: characterization of the In_2S_3/polyaniline and In_2S_3/polypyrrole heterojunctions

E. DALAS, S. SAKKOPOULOS*, E. VITORATOS*, G. MAROULIS
*Department of Chemistry, and *Department of Physics, University of Patras, GR-261 10, Patras, Greece*

L. KOBOTIATIS
Center of Technology and Applications of the Hellenic Air Force, Glyfada Attikis, Greece

The stability of indium sulphide aqueous supersaturated solutions at pH 2.50 and 25 °C was investigated. Spontaneous precipitation proceeded at rates proportional to the solution supersaturation via a polynuclear mechanism and the phase formed was identified as In_2S_3. The absorption spectrum of In_2S_3 was measured from 190–800 nm and from the absorption threshold the optical energy gap was estimated to be $E_0 = (1.8 \pm 0.1)$ eV. The thermal energy gap $E_t = (1.6 \pm 0.2)$eV was determined from resistivity against temperature measurements and a thermopower coefficient $S = -100\ \mu V\ K^{-1}$ at room temperature was found. Finally, In_2S_3/polyaniline and In_2S_3/polypyrrole heterojunctions were prepared and from the investigation of their I–V characteristics, the values of the ideality factor, n, the saturation current density, J_0, and the effective barrier height, φ_B, were determined to be $n = (15 \pm 2)$, $J_0 = (38 \pm 7)\ A\ m^{-2}$ and $\varphi_B = 0.56$ eV for the polyaniline and $n = (64 \pm 8)$, $J_0 = (13 \pm 2)\ A\ m^{-2}$ and $\varphi_B = 0.59$ eV for the polypyrrole heterojunction.

1. Introduction

Metal chalogenides form a very interesting class of compounds because of their photocatalytic properties when irradiated with visible light. Indium sulphide (In_2S_3), usually an n-type semiconductor with an energy gap of approximately 2.0 eV [1], at ambient temperatures shows a defect, cubic structure known as α-In_2S_3, which transforms into a defect spinel, β-In_2S_3, at 420 °C and into a layered structure, γ-In_2S_3, at 740 °C [1–3]. Despite the fact that In_2S_3 shows interesting properties, systematic work concerning its preparation in aqueous media and characterization of polycrystalline preparations was not found in the literature. Characteristics such as particle size of In_2S_3 have been reported to be significant for photocorrosion of this material [4, 5], as well as modifying the band gap [6].

A study of the In_2O_3–H_2S–H_2O system in which the stability regions of the supersaturated solutions were defined and the spontaneously formed solid precipitates were characterized, is reported here.

Recently, increasing interest has been shown in heterojunctions which can convert optical to electrical energy with one of the two materials of the junction a conducting polymer [7, 8]. Conducting polymers are inexpensive and easy to construct and they can be reversibly doped in a way that their electrical conductivity varies continuously from an insulating to a metallic state [9, 10]. Polyaniline and polypyrrole are chemically stable under environmental conditions and they have been recently synthesized and their electrical properties investigated in our Departments [11–13]. These prompted us to construct In_2S_3/polyaniline and In_2S_3/polypyrrole heterojunctions and investigate their I–V characteristics, noting that these have possible applications in photovoltaic electric generators.

2. Experimental procedure

2.1. Crystallization experiments

The experiments were carried out at 25.0 ± 0.1 °C in a 200 cm^3 thermostatted, double-walled cylindrical Pyrex vessel. Triply distilled, carbon dioxide-free water and reagent-grade solid reagents were used for the preparation of stock solutions. Indium chloride (Merck) was used for the preparation of stock indium solutions, which was standardized (at 303.9 nm) by atomic absorption spectroscopy using a Varian 1200 instrument. Ammonium sulphide stock solutions were prepared from the reagent (Merck) and were standardized for sulphide by a titrimetric (iodine) method [14]. Equal volumes of the stock indium chloride and ammonium sulphide solutions, 100 cm^3 each, were prepared and subsequently mixed in the reactor. Both the conductivity and the solution pH were monitored

0022–2461

following the preparation of the supersaturated solution through appropriate sensors fitted in the lid of the reaction vessel.

The pH of the supersaturated solutions was adjusted to the desired value by the controlled addition of 0.1 mol dm^{-3} nitric acid standard solutions (Merk, Titrisol). The time elapsed from mixing the indium and sulphide solutions to the observation of a change in solution conductivity, shown by the change of the slope in the plot of conductivity versus time, was defined as the induction period. The reproducibility was better than 5%. During the course of the reaction, samples were withdrawn and filtered through membrane filters (Sartorious 0.20 μm) and the liquid phase was analysed for indium while the solids were characterized by powder X-ray diffraction (Philips 1300/00) using aluminium as internal standard, by infrared spectroscopy (Perkin–Elmer 477), scanning electron microscopy (Jeol JSM-35) and diffuse reflectance spectroscopy (DRS Shimadzu, Spectronic 210 UV).

2.2. Preparation of the polymers

The deposition of the conducting polymers was carried by polymerization under low pressure (0.1 mm Hg) in a vacuum reactor [15]. Temperature was maintained at 15 °C and the reaction time was 24 h for polyaniline and 5 h for polypyrrole. Prior to deposition of the conducting polymers, the surfaces were treated with 0.1 ml aqueous 35% $FeCl_3$ (Ferrak, Analar). The conducting polymer surface was washed with methanol and dried under vacuum overnight.

2.3. Conductivity measurements

The specimens in the shape of discs, 13 mm diameter and about 1.5 mm thick, were made by pressing indium sulphide powder in an IR press. For the conductivity measurements a centred square four-probe array of electrical contacts, made by pressing tungsten wires against the specimen, was employed [16]. Measurements of the d.c. resistivity against temperature were made in a cryostat containing liquid nitrogen. Thermopower measurements in the range from 280–320 K were carried out in an apparatus described elsewhere [17].

3. Results and discussion

The experimental conditions and the initial rates obtained are summarized in Table I. The solid precipitates collected at the end of precipitation showed the characteristic powder X-ray diffractograms of In_2S_3 [18] (Fig. 1a).

Chemical analysis based on dissolution of precipitated indium sulphide specimens gave an In/S stoichiometry of 0.68 ± 0.08 (mean of twenty specimens). In Fig. 1b the infrared spectrum of the solid precipitates is shown. All subsequent analysis was therefore made with respect to the formation of this solid. The driving force for the formation of In_2S_3 is the average change per ion in the Gibbs energy, ΔG, on going from supersaturated solution to equilibrium

$$\Delta G = -(RT/5)\ln[(In^{3+})^2(S^{2-})^3/Ks^0] \quad (1)$$

$$\Delta G = -(RT/5)\ln\Omega \quad (2)$$

where R is the gas constant, T the absolute temperature, Ks^0 the thermodynamic solubility product of In_2S_3 and the parentheses denote activities. Ω is defined as the supersaturation ratio for non-equivalent solutions, the number of ions in the crystal is 5, while

$$\sigma = \Omega^{1/5} - 1 \quad (3)$$

is the relative supersaturation with respect to the solid phase considered. The computation of the driving force and the solution supersaturation necessitated the calculation of the activities of all ionic species in solution. This was done from the appropriate equilibria summarized in Table II [19], the mass balance equations for total indium, In_t

$$\begin{aligned} In_t = {} & [In^{3+}] + [InCl^{2+}] + [InCl_2^+] + [InCl_3^0] \\ & + [InOHCl^+] + [In_2OHCl^{4+}] + [InOH^{2+}] \\ & + [In(OH)_2^+] + [In(OH)_3] + [In(OH)_4^-] \\ & + [In_3(OH)_4^{5+}] \end{aligned} \quad (4)$$

and for total sulphide, S_t

$$S_t = [S^{2-}] + [HS^-] + [H_2S] \quad (5)$$

By including the electroneutrality condition, the system of equations was solved by successive approximations for the ionic strength [20]. In Equations 4 and 5 the square brackets denote analytical concentrations of the species.

As may be seen from Table I the induction times are inversely proportional to the solution supersaturation and the stability diagram is presented in Fig. 2. The dependence of the rates of precipitation, R, on the relative supersaturation was fitted to the phenomenological equation

$$R = K\sigma^{n_s} \quad (6)$$

TABLE I Spontaneous precipitation of In_2S_3 in aqueous solutions. Total indium, In_t = total sulphide, S_t: pH 2.50, 25 °C

Exp.	$In_t = S_t$ (10^{-4} mol dm^{-3})	ΔG (kJ mol^{-1})	Induction time, τ (min)	Rate (10^5 mol dm^{-3} min^{-1})
1	2.00	− 8.2	4	4.5
2	1.75	− 7.9	10	2.8
3	1.50	− 7.6	30	1.8
4	1.25	− 7.1	112	1.2

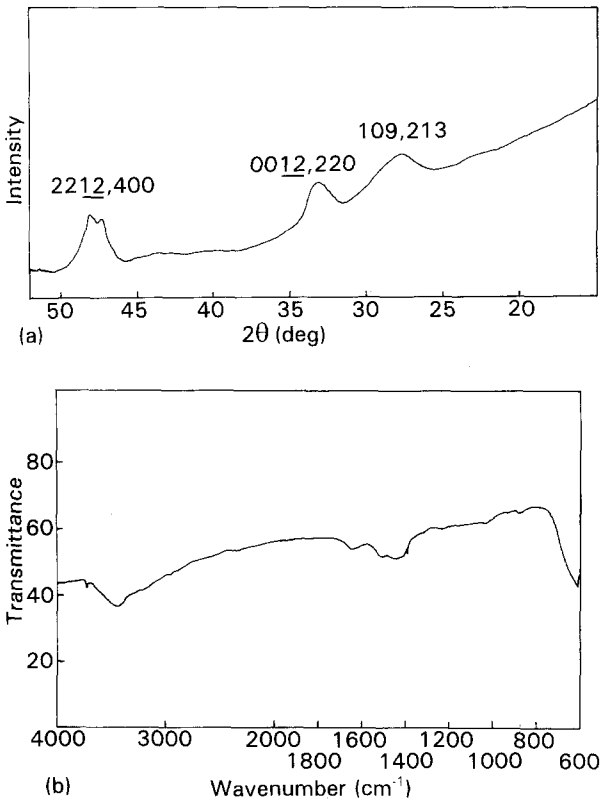

Figure 1 (a) Powder X-ray diffraction spectrum of In_2S_3. (b) Infrared spectrum of In_2S_3 spontaneously precipitated in $InCl_3$–$(NH_4)_2S$ solution.

TABLE II Equilibria for speciation calculation in indium (III) sulphide aqueous solutions at 25 °C.

Equilibrium	Thermodynamic constants [19] log K^0
$InCl^{2+} = In^{3+} + Cl^-$	− 2.32
$InCl_2^+ = In^{3+} + 2Cl^-$	− 3.62
$InCl_3 = In^{3+} + 3Cl^-$	− 4.00
$InOHCl^+ = InCl^{2+} + OH^-$	− 10.30
$In_2OHCl^{4+} = InOHCl^+ + In^{3+}$	− 1.60
$InOH^{2+} = In^{3+} + OH^-$	− 10.00
$In(OH)_2^+ = In^{3+} + 2OH^-$	− 20.20
$In(OH)_3 = In^{3+} + 3OH^-$	− 29.60
$In(OH)_4^- = In^{3+} + 4OH^-$	− 33.90
$In_3(OH)_4^{5+} = 3In^{3+} + 4OH^-$	− 50.20
$In_2S_3(s) = 2In^{3+} + 3S^{2-}$	− 69.40

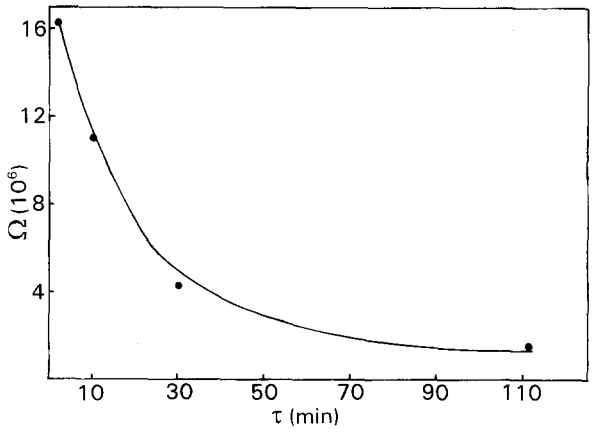

Figure 2 Stability diagram for the $InCl_3$–$(NH_4)_2S$ system, pH 2.50, 25 °C.

in which K and n_s are constants. A logarithmic plot according to Equation 6 yielded a straight line shown in Fig. 3. From the slope of the line, a value of $n_s = 3.0 \pm 0.2$ was obtained. Similar values have been obtained for other spontaneously precipitating systems [21–23]. The high value of n_s is probably due to the fact that initial rates are considered. At this point both nucleation (high values of n_s) and crystal growth ($n_s = 1$ or 2) are operative. Typical scanning electron micrographs of spontaneously precipitated In_2S_3 are shown in Fig. 4.

Fig. 5 shows the absorption spectrum of In_2S_3 precipitates. The energy gap evaluated from the absorption threshold was 1.8 eV. In_2S_3 specimens in the shape of discs, 13 mm diameter and about 1.5 mm thick, were heated at 250 °C at a heating rate of 10 K min^{-1} for 1.5 min in a tube furnace with a nitrogen flow rate of 250 cm^3 min^{-1}. Further investigation of the electronic properties of the In_2S_3 was done by measuring the resistivity of the preheated In_2S_3 discs, as a function of temperature. A diagram of ln ρ against $1/T$ is shown in Fig. 6. As one can observe from this diagram, the resistivity remains almost constant below approximately 330 K, although at higher temperatures an exponential decrease of resistivity with increasing T is observed. This is typical behaviour of a heavily doped semiconductor, in which impurity-band conduction takes place at $T < 330$ K before thermal excitation of carriers results in the exponential intrinsic conduction region [24]. From the slope of the latter a thermal energy gap $E_g = (1.6 \pm 0.2)$ eV is deduced.

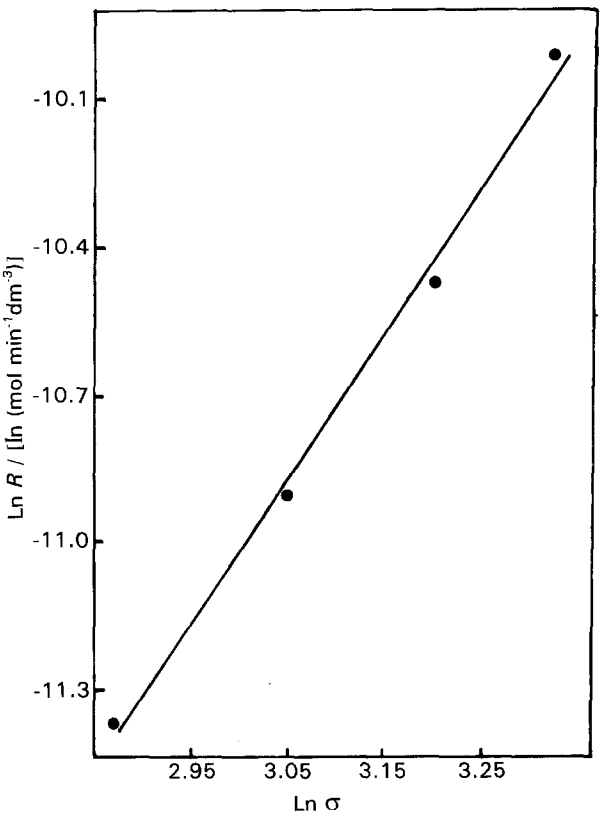

Figure 3 Spontaneous precipitation of In_2S_3 in aqueous solutions, pH 2.50, 25 °C.

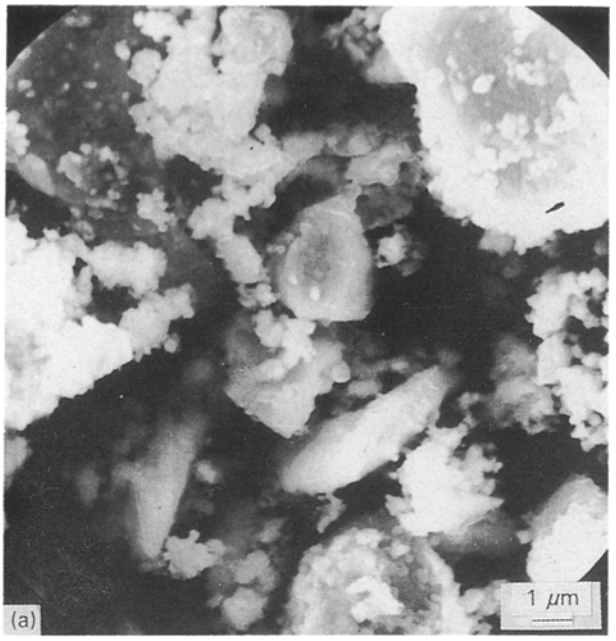

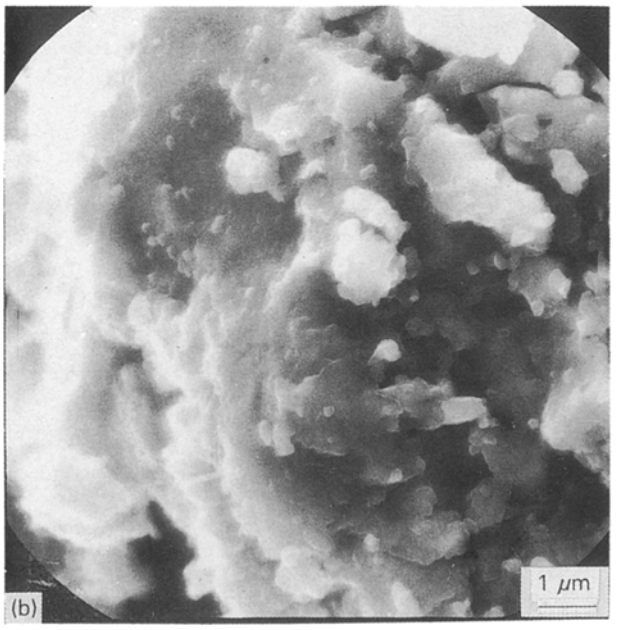

Figure 4 Scanning electron micrographs of spontaneously precipitated In_2S_3.

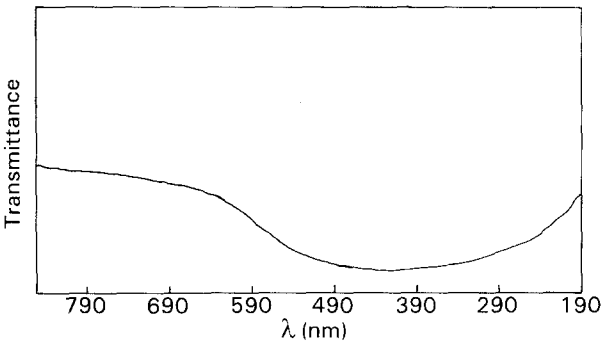

Figure 5 Absorption spectra of In_2S_3 precipitations.

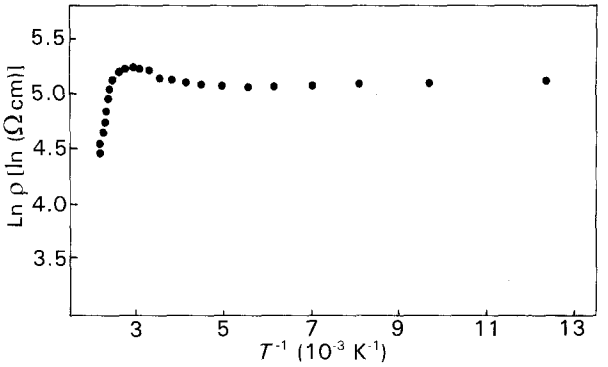

Figure 6 Plot of $\ln \rho$ as a function of $1/T$ for In_2S_3.

The thermopower of the specimens was about $-100\ \mu V\ K^{-1}$ in the temperature range 280–320 K, typical for an n-type semiconductor.

Polyaniline and polypyrrole exhibit a thermally activated conductivity, following the equation $\sigma = \sigma_0 \exp[-(T_0/T)^n]$, where σ_0 and T_0 are quantities almost independent of temperature and determined mainly by the polymer and the dopand. The exponent n takes the values $\frac{1}{2}$ for polyaniline and $\frac{1}{4}$ for polypyrrole [25, 26] indicating conduction by tunnelling of carriers between "metallic" regions in the first and by variable-range hopping in three dimensions in the second polymer.

The fibril structure of the polymers makes them non-homogeneous and the change of their conductivity is governed almost exclusively by the interchain hopping of the carriers, polarons in polyaniline and bipolarons in polypyrrole. At room temperature the conductivity of polyaniline and polypyrrole is about $16\ \Omega^{-1}\ cm^{-1}$ compared to $5.2 \times 10^{-3}\ \Omega^{-1}\ cm^{-1}$ for In_2S_3. The thermopower, on the other hand, depends mainly on the intrachain conduction [9] and at room temperature takes the values $S = -50\ \mu V\ K^{-1}$ and $20\ \mu V\ K^{-1}$ for polyaniline and polypyrrole respectively [12, 13].

In Fig. 7a and b, the I–V characteristics of the In_2S_3/polypyrrole and In_2S_3/polyaniline are shown, respectively [27, 28]. The difference between the work functions of In_2S_3 and the two conducting polymers creates a potential barrier across the junction. The electric field into this barrier is essential for the operation of the heterojunction as a photovoltaic cell. For the In_2S_3/polypyrrole, the forward bias corresponds to an external electric field from polypyrrole to In_2S_3. This is justified by the fact that polypyrrole has a high work function $\varphi_{PA} = 4.8$ eV [7], and receives electrons from In_2S_3. The opposite happens for the In_2S_3/polyaniline heterojunction.

The I–V characteristics can be understood according to the theory of metal–semiconductor barriers [29, 30]. When thermionic and thermionic field emission are present, the current is

$$J = J_0 \exp(qV/nkT)[1 - \exp(qV/kT)] \quad (7)$$

where J is the total current, J_0 the saturation current, q the electron charge, V the applied voltage and n the ideality factor. The saturation current, J_0, across the potential barrier has the form

$$J_0 = AT^2 \exp(-\varphi_B/kT) \quad (8)$$

where A is the Richardson constant, and φ_B the effective barrier that carriers must overcome to cross the heterojunction.

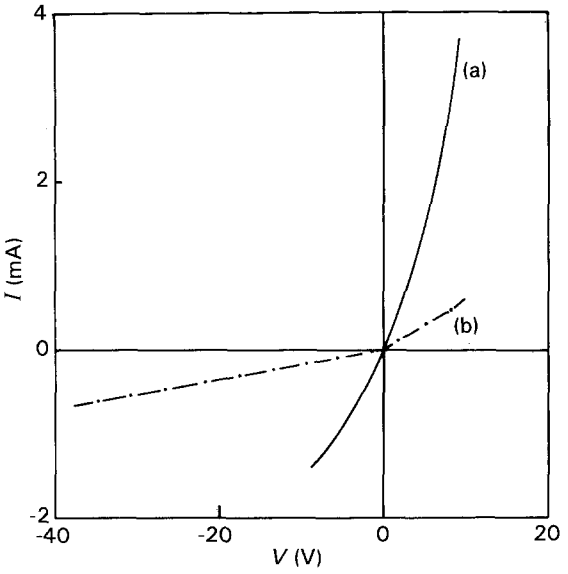

Figure 7 I–V characteristics of (a) In_2S_3/polypyrrole, and (b) In_2S_3/polyaniline heterojunctions.

Fitting of the experimental data by Equation 7 using multidimensional non-linear regression on a IBM/386 microcomputer, yielded the values $n = (64 \pm 8)$ and $J_0 = (13 \pm 2)\,Am^{-2}$ for the In_2S_3/polypyrrole heterojunction and the values $n = (15 \pm 2)$ and $J_0 = (38 \pm 7)\,Am^{-2}$ for the In_2S_3/polyaniline heterojunction.

From Equation 8 the barrier height can be estimated. Taking $A = 1.2 \times 10^6\,Am^{-2}K^{-2}$ and the values of J_0 obtained from the I–V curve fitting, we get $\varphi_{B1} = 0.59$ eV for $\varphi_{B2} = 0.56$ eV for the In_2S_3/polypyrrole and the In_2S_3/polyaniline, respectively. These are close to the values of φ_B ranging from 0.68–0.9 eV obtained for polypyrrole on n-Si/Pt and α-Si: H, deduced from I–V, C–V and internal photoemission [7].

The real barrier height must be higher than the calculated values of φ_{b1} and φ_{b2}, because the real contact area is expected to be smaller than the geometrical, because of the fibrillar, non-homogeneous structure of the polymers. Moreover, the high values of n obtained (usually between 1 and 4) indicate that probably a thin interfacial insulating layer is present, which decreases the effective barrier height and causes the inverse current to fail to reach saturation [29]. Besides, A in Equation 8 was taken equal to the Richardson constant, not corrected by the factor m^*/m, where m^* is the conduction band mass of the electrons in In_2S_3 and m the free electron mass [8].

4. Conclusions

In this paper the stability regions of supersaturated In_2O_3–H_2S–H_2O solutions were defined and the spontaneously formed solid precipitate was identified as In_2S_3. This was found to be an n-type semiconductor, with an optical energy gap $E_0 = (1.8 \pm 0.1)$ eV, a thermal energy gap $E_g = (1.6 + 0.2)$ eV and a thermopower coefficient $S = -100\,\mu V\,K^{-1}$ at $T = 300$ K, as deduced from resistivity and thermopower measurements.

In_2S_3/polyaniline and In_2S_3/polypyrrole heterojunctions were fabricated and their I–V characteristics were analysed by the standard Schottky barrier theory. The effective barrier height, saturation current and ideality factor were determined as 0.56 eV $(38 \pm 7)\,A\,m^{-2}$, $n = (15 \pm 2)$ for the In_2S_3/polyaniline and 0.59 eV, $(13 \pm 2)\,A\,m^{-2}$, $n = (64 \pm 8)$ for the In_2S_3/polypyrrole heterojunction.

References

1. J. M. GILES, H. HATWELL, G. OFFERGELD and J. VAN CAKENBERGHE, *J. Phys. Status Solidi* **2** (1962) K73.
2. W. RENWALD and G. HARBEKE, *J. Phys. Chem. Solids* **26** (1966) 1309.
3. G. F. S. GARLIC, M. SPRINGFORD and H. CHECINSKA, *Proc. Phys. Soc. Lond.* **82** (1963) 16.
4. R. ROSETTI, S. NAKAHARE and L. E. BRUS, *J. Chem. Phys.* **79** (1983) 1086.
5. F. WILLIAMS and A. J. NOZIK, *Nature* **311** (1984) 21.
6. H. MIYOSHI, M. YAMACHIKA, H. YONEYAMA and H. MORI, *J. Chem. Soc. Faraday Trans.* **86** (1990) 815.
7. O. INGANAS, T. SKOTHEIM and I. LUNDSTROM, *Phys. Scripta* **25** (1982) 863.
8. A. J. FRANK, S. GLENIS and A. J. NELSON, *J. Phys. Chem.* **93** (1989) 3818.
9. A. J. HEGER, S. KIVELSON, J. R. SCHRIEFFER and W. P. SU, *Rev. Mod. Phys.* **60** (1988) 781.
10. R. H. BAUGHMAN, J. L. BREDAS, R. R. CHANCE, R. L. ELSENBAUER and L. W. SHACKLETTE, *Chem. Rev.* **82** (1982) 209.
11. J. KALLITSIS, E. KOUMANAKOS, E. DALAS, S. SAKKOPOULOS and P. G. KOUTSOUKOS, *J. Chem. Soc. Chem. Commun.* **16** (1989) 1146.
12. E. DALAS, S. SAKKOPOULOS, J. KALLITSIS, E. VITORATOS and P. G. KOUTSOUKOS, *Langmuir* **6** (1990) 1356.
13. S. SAKKOPOULOS, E. VITORATOS, E. DALAS, G. PANDIS and D. TSAMOURAS, *J. Phys. Condens. Matter* **4** (1992) 2231.
14. J. H. KARCHNIER, "The Analytical Chemistry of Sulphur and its Compounds", Part I (Wiley, New York, 1970).
15. E. DALAS, *Solid State Commun.* **77** (1991) 63.
16. H. H. WIEDER, "Laboratory Notes of Electrical and Galvanomagnetic Measurements" (Elsevier, Amsterdam, 1979).
17. K. LARK-HOROVITZ and V. A. JOHNSON, "Methods of Experimental Physics (Solid State Physics)", Vol. 6, Part A (Academic Press, New York, 1959) p. 403.
18. ASTM card file no. 25-390 (American Society for Testing and Materials, Philadelphia, PA).
19. R. M. SMITH and A. E. MARTELL, "Critical Stability Constants", Vol. 3 (Plenum Press, New York, 1976).
20. C. W. DAVIES, "Ion Association" (Butterworths, Washington, 1962).
21. E. DALAS and P. G. KOUTSOUKOS, *Desalination* **78** (1990) 403.
22. *Idem, Geothermics* **18** (1989) 83.
23. E. KOUMANAKOS, E. DALAS and P. G. KOUTSOUKOS, *J. Chem. Soc. Faraday Trans.* **86** (1990) 973.
24. F. J. BLATT, "Physics of Electronic Conduction in Solids" (McGraw-Hill, New York, 1968).
25. Y. M. PARK, Y. S. LEE, C. PARK, L. W. SCHACKLETTE and R. H. BAUGHMAN, *Solid State Commun.* **63** (1987) 1063.
26. T. A. EZQUERRA, J. RUHE and G. WEGNER, *Chem. Phys. lett.* **144** (1988) 194.
27. A. WATANABE, S. MURAKAMI, K. MORI and Y. KASHIWABA, *Macromolecules* **22** (1989) 4231.
28. S. MIYAUCHI, Y. GOTO, I. TSUBATA and Y. SORIMACHI, *Synth. Metals* **41–43** (1991) 1051.
29. E. H. RHODERICK, "Metal-semiconductor contacts" (Clarendon Press, Oxford, 1980).
30. V. L. RIDEOUT, *Solid-State Electron.* **18** (1975) 541.

Received 20 January
and accepted 3 February 1993